Physica Medica 60 (2019) 83–90

Contents lists available at ScienceDirect

Physica Medica

journal homepage: www.elsevier.com/locate/ejmp

Original paper

# Volumetric modulated arc therapy planning based on virtual monochromatic images: Effect of inaccurate CT numbers on dose distributions

Shingo Ohira[a,b,*], Riho Komiyama[a], Tsukasa Karino[a], Hayate Washio[a], Yoshihiro Ueda[a], Masayoshi Miyazaki[a], Masahiko Koizumi[b], Teruki Teshima[a]

[a] Department of Radiation Oncology, Osaka International Cancer Institute, Osaka, Japan
[b] Department of Medical Physics and Engineering, Osaka University Graduate School of Medicine, Suita, Japan

ARTICLE INFO

*Keywords:*
Dual-energy CT
Volumetric modulated arc therapy
Virtual monochromatic image

ABSTRACT

*Purpose:* Though virtual monochromatic images (VMIs) at low energy levels can improve image quality, the measured Hounsfield unit (HU) values can be inaccurate. We assessed the dosimetric error due to inaccurate HU estimation in volumetric modulated arc therapy (VMAT) planning.

*Methods:* Based on the VMIs at 50 keV ($VMI_{50keV}$), 77 keV ($VMI_{77keV}$) and single-energy CT (SECT) image for a phantom with different sizes, lookup tables ($LUT_L$ and $LUT_S$) were created. Using an anthropomorphic phantom (head and spine regions), VMAT plans were generated based on $VMI_{50keV}$, $VMI_{77keV}$ and SECT using the corresponding $LUT_L$, and then, the doses were re-calculated using $LUT_S$. For clinical cases, 30 VMAT plans (prostate, brain, and spine cases) were generated based on $VMI_{50keV}$ and $VMI_{77keV}$.

*Results:* In the anthropomorphic phantom study, the difference in the dosimetric parameters for planning target volume (PTV) in the VMAT plan based on the $VMI_{77keV}$ was smallest (within 0.1 Gy) among three types of treatment planning approach. In clinical cases, in general, the differences of the 3-dimensional gamma passing rate and dosimetric parameters in the treatment plans based on the $VMI_{50keV}$ were larger than those in the $VMI_{77keV}$. Especially for brain cases, the difference for PTV was more prominent when AXB was used (the maximum difference was 0.5 Gy) than AAA.

*Conclusions:* The dosimetric error due to the inaccurate HU estimation was larger in the VMIs at low energy levels. This may be clinically insignificant, but should be avoided in the VMAT treatment planning.

## 1. Introduction

In modern radiotherapy, the volumetric modulated arc therapy (VMAT) irradiation technique, which involves continuously varying the gantry rotation speed, multi-leaf collimator (MLC) pattern, and dose rate during delivery, has become increasingly common in clinical practice [1–3]. High doses to the target, while minimizing the doses to organs at risk (OAR) is to be expected of any highly conformal radiotherapy. For such sophisticated treatment techniques, computed tomography (CT) simulations play an important role in achieving accurate target delineation and evaluating doses for the targets as well as surrounding OARs.

Recent advancements in CT scanner technology have led to the development and clinical use of dual-energy CT (DECT) that utilizes two different photon beams for its operation; one of the advantage of the DECT scanner is that it can be used to generate virtual monochromatic images (VMIs) at a specified photon energy levels for both high and low photon energies [4]. Several researchers have demonstrated that VMIs obtained at low energy levels (40–60 keV) provided significantly higher image quality for various tumor sites compared with VMIs at high energy levels (70–77 keV), where the energy levels were equivalent to the conventional single polychromatic images (i.e., at 120 kVp) [5–7]; this improvement in image quality has the potential for improving inter- and/or intra-observer variations when determining gross tumor volume in radiotherapy treatment planning.

However, some previous studies showed that the CT numbers (Hounsfield unit; HU) in the case of VMIs at low energy level could be considerably inaccurate, especially for high-density materials; in

*Abbreviations:* DECT, dual-energy CT; VMI, virtual monochromatic image; SECT, single-energy CT; LUT, lookup table

* Corresponding author at: Department of Radiation Oncology, Osaka International Cancer Institute, 3-1-69 Otemae, Chuo-ku, Osaka 537-8567, Japan.
*E-mail address:* oohira-si@mc.pref.osaka.jp (S. Ohira).

https://doi.org/10.1016/j.ejmp.2019.03.022
Received 9 October 2018; Received in revised form 15 March 2019; Accepted 20 March 2019
Available online 29 March 2019

**Table 1**
Specification of the reference materials.

| Reference material # | Rod material | Electron density relative to water | Physical density (g/cm$^3$) |
|---|---|---|---|
| 1 | LN-300 Lung | 0.278 | 0.290 |
| 2 | LN-450 Lung | 0.455 | 0.470 |
| 3 | AP6 Adipose | 0.932 | 0.949 |
| 4 | BR-12 Breast | 0.960 | 0.983 |
| 5 | Water Insert | 1.000 | 1.000 |
| 6 | CT Solid Water 1 | 0.987 | 1.016 |
| 7 | CT Solid Water 2 | 0.987 | 1.016 |
| 8 | CT Solid Water 3 | 0.987 | 1.016 |
| 9 | BRN-SR2 Brain | 1.047 | 1.051 |
| 10 | LV1 Liver | 1.060 | 1.091 |
| 11 | IB Inner bone | 1.096 | 1.143 |
| 12 | B200 Bone mineral | 1.104 | 1.152 |
| 13 | CB2-30% CaCO3 | 1.277 | 1.332 |
| 14 | CB2-50% CaCO3 | 1.469 | 1.559 |
| 15 | SB3 Cortical Bone | 1.694 | 1.822 |
| 16 | Aluminum 1100 | 2.360 | 2.710 |

addition, the accuracy of the HU values varied based on the volume of the surrounding tissues [8,9]. In general, the CT numbers (Hounsfield unit, HU) are converted into electron and physical density values by using lookup tables (LUTs) for dose calculation in the radiotherapy treatment planning processes to account for inhomogeneous environments in patient anatomy. It is a common practice to register the LUT acquired using a commercial phantom for a corresponding CT scanner in a treatment planning system; thus, the use of VMIs obtained at low energy levels for VMAT planning might induce unexpected dosimetric errors during the dose calculation process because of the inaccurate estimation of HU values. To the best of our knowledge, no previous studies have investigated the effect of inaccurate HU estimation on dose distributions in VMAT planning.

Our study consisted of two components. First, we assessed the variance of HU measurements in the VMIs at 50 keV ($VMI_{50keV}$; high contrast image) and 77 keV ($VMI_{77keV}$; equivalent HU values for a conventional 120 kVp CT image) and single-energy CT (SECT) images with different phantom sizes. Second, we compared the effect of the inaccuracy of HU estimation for VMAT planning in an anthropomorphic phantom and patients.

## 2. Materials and Methods

### 2.1. Generation of LUTs

We used a 16.5-cm-deep multi-energy phantom (Gammex RMI 1472; Gammex RMI, Middleton, WI), which consisted of inner (20 cm in diameter) and outer (40 cm in width and 30 cm in height) sections composed of a water-equivalent material to simulate large and small patient sizes. The phantom contained cylindrical holes (2.85 cm in diameter) to enable the placement of various rods of the reference materials to be tested. In our study, 16 reference materials for a tissue characterization phantom (Gammex RMI 467; Gammex RMI) were inserted in the multi-energy phantom specified earlier. To extend the usable region of the LUT in our work, Al was used as one of the reference materials. Table 1 lists the specifications of the reference materials used in our study; these specifications were provided by the manufacturer. The phantoms with large and small sizes were scanned using a single-source DECT scanner with rapid kilovolt peak switching (Revolution HD; GE Medical Systems, Milwaukee, WI). To generate the LUTs, the dual-energy scan (protocol number #1 in Table 2) and the single-energy scan (protocol number #9 in Table 2) were repeated five times to reduce the effect of random variations on data measurements. Subsequently, various scanning parameters (protocol number #1–16 in Table 2) were applied, and scans were repeated three times for each protocol to investigate the effect of the scanning parameters on the quantitative measurements.

The acquired data sets were transferred to a workstation (Advantage Sim, GE Medical Systems), using which the $VMI_{50keV}$ and $VMI_{77keV}$ were reconstructed using the projection-based method. We considered the HU values in the $VMI_{77keV}$ are equivalent with that in the conventional CT image with 120 kVp because the HU values between these two images in the tissue characterization phantom (GAMMEX RMI 467) are almost perfectly coincident in our previous work [10]. A circular region of interest of 20-mm diameter was placed at the center of each reference material on the VMIs. Further, the quantitative data obtained using the phantom images (both large and small phantom sizes) were used to create LUTs to convert the measured HU values of the VMIs ($LUT_{50L}$, $LUT_{50S}$, $LUT_{77L}$, and $LUT_{77S}$) and SECT ($LUT_{SECTL}$ and $LUT_{SECTS}$) images to electron and physical density values. The effect of the scanning parameters on the quantitative measurements was evaluated as the standard deviation (SD) of repeated measurements for each protocol in Table 2.

**Table 2**
Scanning protocols.

| Protocol number # | Type of scanning field of view | Field of view | Beam collimation (mm) | Gantry rotation time (s/rot) | Helical pitch | Tube current (mA) | $CTDI_{vol}$ (mGy) | Tube voltage (kVp) | Scanning mode | Slice thickness (mm) |
|---|---|---|---|---|---|---|---|---|---|---|
| *Dual-energy scan* | | | | | | | | | | |
| 1 | Large body | 500 | 40 | 1.0 | 0.984 | 600 | 32.52 | 80/140 | Helical | 2 |
| 2 | Large body | 500 | 40 | 0.7 | 0.984 | 260 | 9.05 | | | |
| 3 | Medium body | 500 | 40 | 1.0 | 0.984 | 600 | 33.96 | | | |
| 4 | Medium body | 500 | 40 | 0.6 | 0.984 | 275 | 9.66 | | | |
| 5 | Medium head | 320 | 20 | 0.9 | 0.969 | 600 | 72.65 | | | |
| 6 | Medium head | 320 | 20 | 0.8 | 0.969 | 260 | 26.22 | | | |
| 7 | Small head | 320 | 20 | 0.5 | 0.969 | 630 | 39.66 | | | |
| 8 | Small head | 320 | 20 | 0.8 | 0.969 | 260 | 23.12 | | | |
| *Single-energy scan* | | | | | | | | | | |
| 9 | Large body | 500 | 40 | 1.0 | 0.984 | 400 | 32.60 | 120 | Helical | 2 |
| 10 | Large body | 500 | 40 | 0.7 | 0.984 | 160 | 9.13 | | | |
| 11 | Medium body | 500 | 40 | 1.0 | 0.984 | 400 | 33.75 | | | |
| 12 | Medium body | 500 | 40 | 0.6 | 0.984 | 190 | 9.62 | | | |
| 13 | Medium head | 320 | 20 | 0.9 | 0.969 | 390 | 72.33 | | | |
| 14 | Medium head | 320 | 20 | 0.8 | 0.969 | 160 | 26.38 | | | |
| 15 | Small head | 320 | 20 | 0.5 | 0.969 | 430 | 39.48 | | | |
| 16 | Small head | 320 | 20 | 0.8 | 0.969 | 155 | 22.77 | | | |

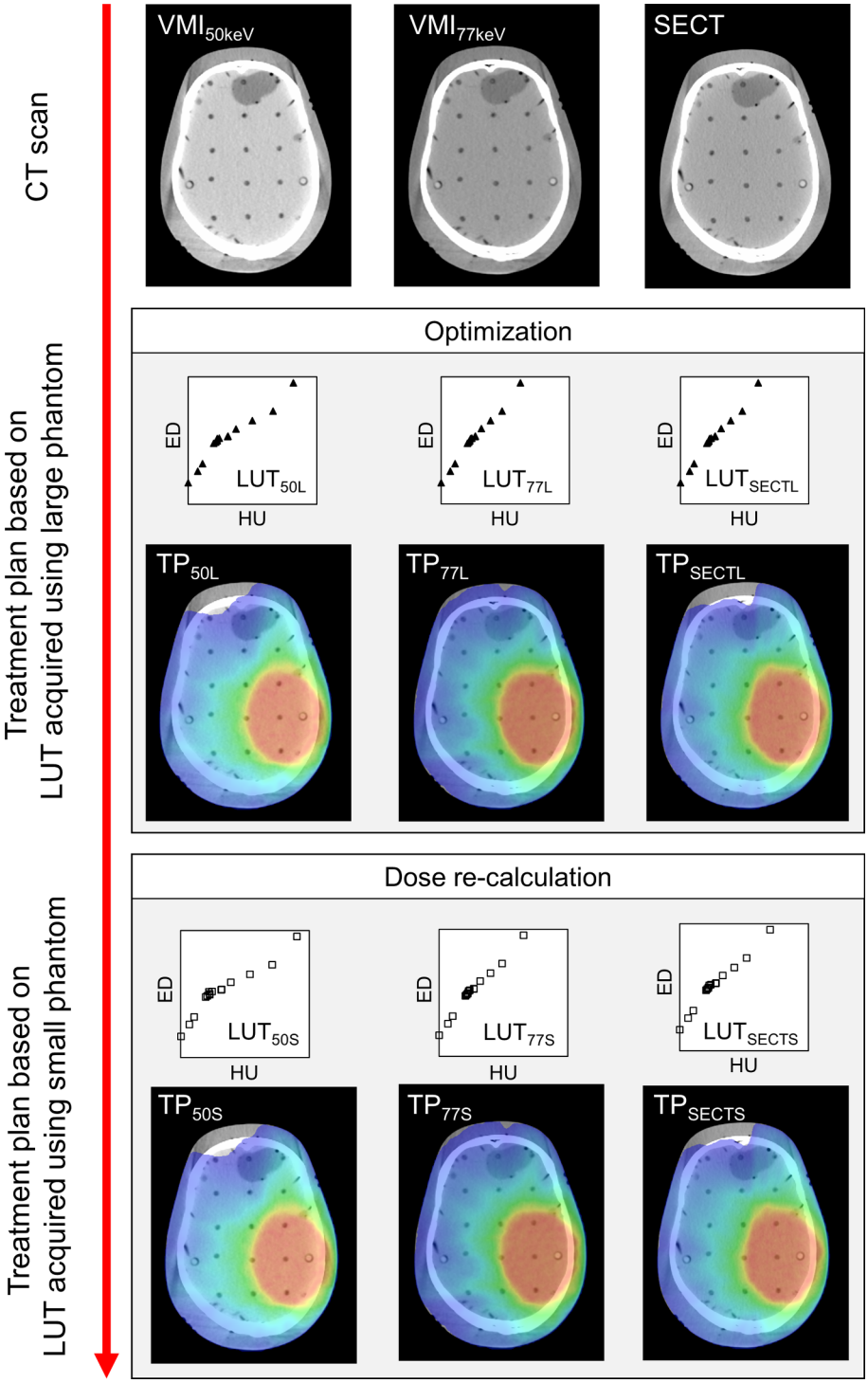


**Fig. 1.** Schematic workflow that is used to investigate the effect of inaccurate HU estimation on dose distributions in VMAT planning.

### 2.2. VMAT planning for anthropomorphic phantom

In accordance with our clinical settings, VMAT treatment plans were generated using an anthropomorphic phantom (Alderson Rando phantom, Alderson Research Laboratories, Stamford, CT) of the head and spine (thorax) regions. The prescription dose for the planning target volume (PTV) in the head and spine region was 60 and 25 Gy, respectively. Fig. 1 shows the schematic workflow used in this study to investigate the effect of inaccurate HU estimation on dose distributions in VMAT planning. The VMAT plans were generated based on $VMI_{50keV}$, $VMI_{77keV}$ and SECT; furthermore, $LUT_{50L}$, $LUT_{77L}$ and $LUT_{SECTL}$ were used for the dose calculation process. Doses of the resultant treatment plans obtained using $VMI_{50keV}$ ($TP_{50L}$), $VMI_{77keV}$ ($TP_{77L}$) and SECT ($TP_{SECTL}$) were re-calculated using $LUT_{50S}$, $LUT_{77S}$ and $LUT_{SECTS}$ with all planning parameters (dose calculation algorithm, beam arrangement, leaf motion, number of monitor units, etc.) remaining consistent. All treatment plans were generated using a treatment planning system (Eclipse version 13.7; Varian Medical Systems, Palo Alto, CA) with a 6-MV photon beam energy. Furthermore, the doses were calculated using an anisotropic analytical algorithm (AAA) and Acuros XB (AXB) with a grid size of 2 mm. The absolute difference in dosimetric parameter was determined by subtracting the dosimetric parameters of the planning

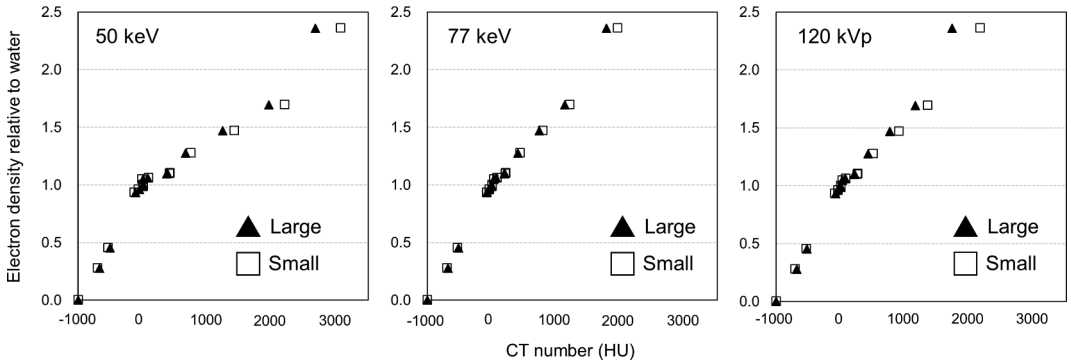


**Fig. 2.** Lookup tables generated from VMI at 50 keV and 77 keV, and single-energy CT image (120kVp) using different phantom sizes.

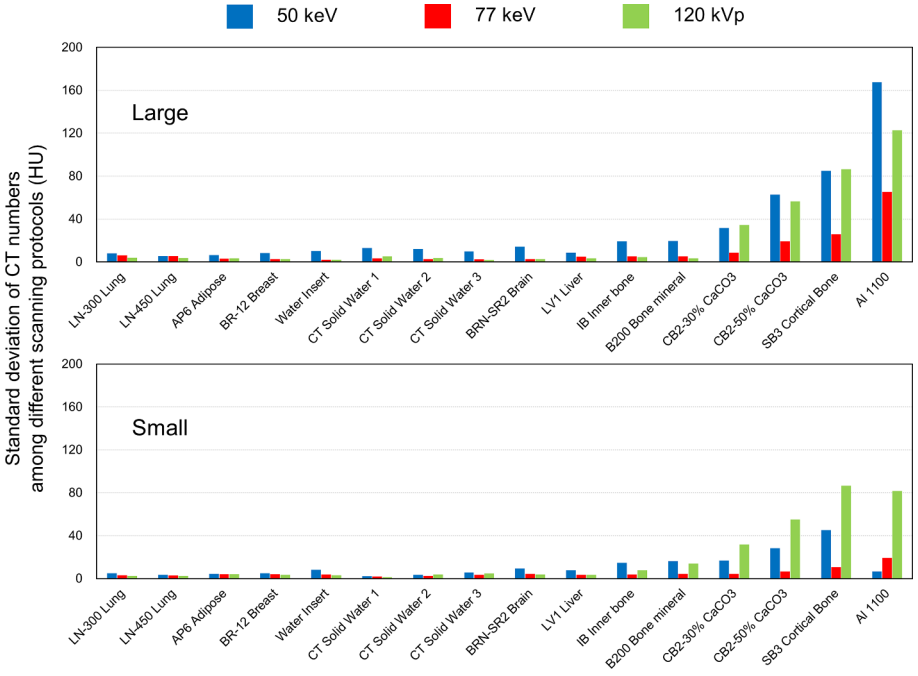


**Fig. 3.** Effect of the scanning parameters on the quantitative measurements of CT numbers.

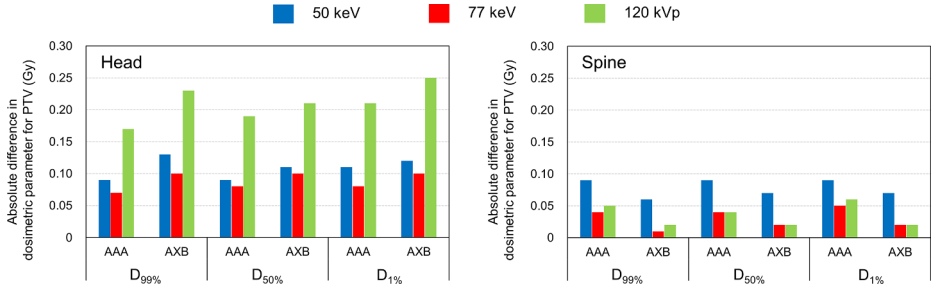


**Fig. 4.** Effect of the inaccurate CT number on VMAT plans in anthropomorphic phantom. $D_{99\%}$, $D_{50\%}$ and $D_{1\%}$ indicate dose receiving 99%, 50% and 1% of PTV volume, respectively.

target volume (PTV) in $TP_{50L}$, $TP_{77L}$ and $TP_{SECTL}$ from those in $TP_{50S}$, $TP_{77S}$ and $TP_{SECTS}$.

### 2.3. VMAT planning for patients

This retrospective study included 30 patients (10 patients with prostate cancer, 10 with brain tumor, and 10 with spine metastases) who underwent VMAT treatment at our institution. This study was approved by our ethics committee, and written informed consent was obtained from each patient. All patients underwent the DECT simulations. For patients with brain tumor, an intravenous contrast-enhanced agent was injected for the delineation of targets; in clinical practice, $VMI_{77keV}$ was used for VMAT planning to deliver prescription doses of 78 Gy, 60 Gy, and 25–35 Gy for the PTV in the case of prostate cancer (body region), brain tumor (head region), and spine metastases plans (high density target), respectively.

The difference in doses for PTV and OARs between treatment plans based on VMI ($TP_{50L}$ versus $TP_{50S}$ and $TP_{77L}$ versus $TP_{77S}$) were compared. The three-dimensional (3D) gamma analysis based on local dose was performed with the evaluation criteria of 1%/1 mm with a low-

**Table 3**
CT numbers of the target and OARs in the VMIs at 50 and 77 keV.

| Structure | 50 keV (HU) | | 77 keV (HU) | | *p*-value |
|---|---|---|---|---|---|
| | Mean | SD | Mean | SD | |
| Prostate ($n$ = 10) | | | | | |
| PTV | 25.5 | 10.5 | 22.3 | 6.9 | 0.07 |
| Bladder | 17.0 | 13.5 | 7.0 | 9.6 | < 0.01 |
| Rectum | −11.6 | 53.0 | −21.1 | 54.3 | < 0.01 |
| Brain ($n$ = 10) | | | | | |
| PTV | 116.4 | 51.3 | 67.9 | 25.4 | < 0.01 |
| Brainstem | 48.1 | 4.5 | 30.2 | 1.3 | < 0.01 |
| Chiasm | 40.4 | 6.5 | 25.0 | 4.4 | < 0.01 |
| Spine ($n$ = 10) | | | | | |
| PTV | 282.3 | 96.2 | 160.5 | 55.8 | < 0.01 |
| Spinal cord | 51.6 | 10.9 | 33.7 | 7.2 | < 0.01 |
| Esophagus | −4.8 | 53.0 | −16.7 | 50.1 | 0.02 |

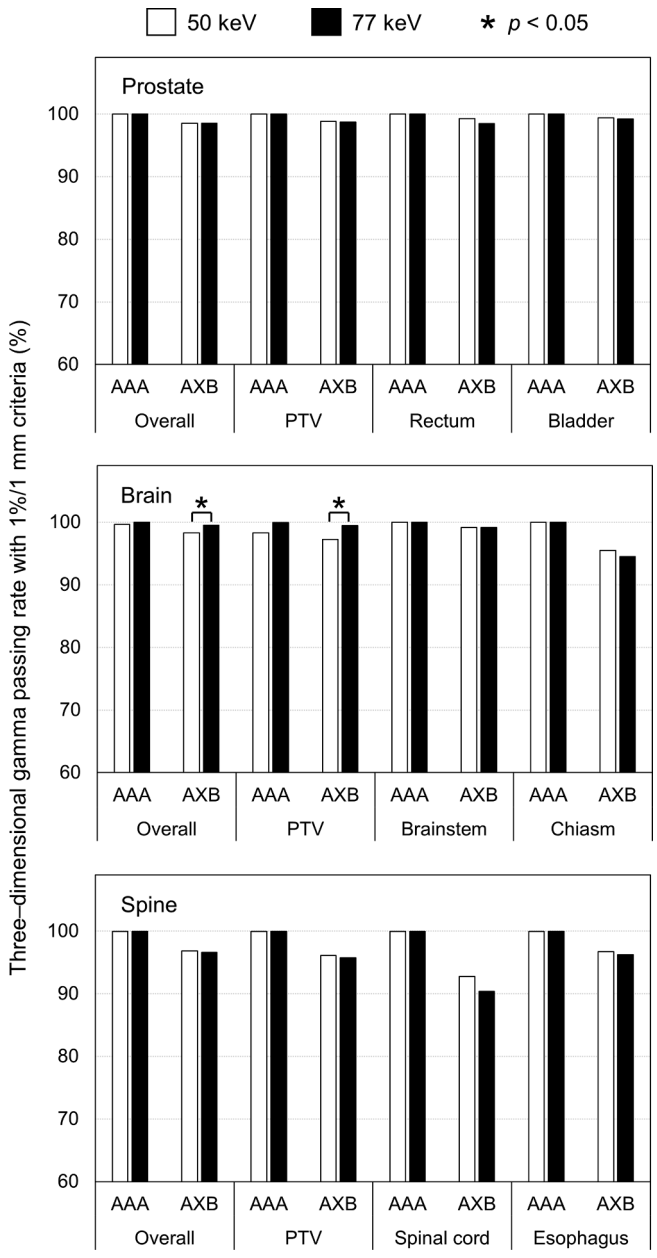


**Fig. 5.** Mean 3D-GPR derived from doses computed based on the LUTs generated using the large phantom size and those using the small phantom size.

dose threshold of 10% [11]. The 3D gamma passing rate (3D–GPR) was defined as the percentage of points satisfying the condition that the gamma index was < 1. Subsequently, the absolute difference in dosimetric parameter was determined by subtracting the dosimetric parameters of the PTV as well as OARs in $TP_{50L}$ and $TP_{77L}$ from those in $TP_{50S}$ and $TP_{77S}$. The discrepancies were expressed as a dose for the PTV, brainstem, chiasm, spinal cord, and esophagus, and as percentage volume of organ for the rectum and bladder. Statistical analysis was performed using the paired Wilcoxon signed-rank test (IBM SPSS Statistics version 24; IBM, Armonk, NY, USA). A $p$-value of < 0.05 was considered to indicate statistical significance.

## 3. Results

Fig. 2 shows the LUTs (electron density) generated from $VMI_{50keV}$, $VMI_{77keV}$ and SECT image. In particular, for high-density materials (electron density > 1.1), $VMI_{50keV}$ provided higher HU values than $VMI_{77keV}$ and SECT. Furthermore, the differences in the absolute (relative) HU value in the case of $VMI_{50keV}$ between the large and small phantoms were 179.9 (14.5%), 240.4 (12.3%), and 389.2 (14.5%) HU for the reference materials of CB2-50%, SB3, and Al, respectively, while these differences in the case of $VMI_{77keV}$ were 57.6 (7.8%), 76.8 (6.8%), and 174.1 HU (9.8%), respectively. For SECT, these differences were 142.7 (18.7%), 188.4 (16.3%) and 436.6 HU (25.3%) for CB2-50%, SB3, and Al, respectively. Fig. 3 shows the effect of the scanning parameters on the quantitative measurements of HU values using different scanning protocols. In the large phantom, the measured HU values were varied widely depending on the scanning protocols than those in the small phantom. The maximum SD in the $VMI_{50keV}$ and SECT image were 167.7, 122.8 HU in the large phantom while that in the $VMI_{77keV}$ was 65.2 HU.

Fig. 4 shows the effect of the inaccurate CT number on the dosimetric parameters in the anthropomorphic phantom. For the head region, the absolute difference in dosimetric parameter was largest in the treatment plan based on the SECT, and the maximum difference was 0.25 Gy ($D_{1\%}$) when AXB was used. For the spine region, the maximum differences of 0.09 Gy was observed in the treatment plan based on the $VMI_{50keV}$. With regard to the treatment plan based on the $VMI_{77keV}$, the difference was smallest among three types of treatment planning approach, and the maximum difference was within 0.10 Gy for all evaluated parameters.

Table 3 lists the HU values in $VMI_{50keV}$ and $VMI_{77keV}$ for the prostate, brain, and spine cases. For almost all structures, $VMI_{50keV}$ provided significantly higher HU values ($p$ < 0.05) than the corresponding values in $VMI_{77keV}$. In the cases of the spine, the PTV involved high-density structures and HU values were highest (282.3 ± 96.2 HU for $VMI_{50keV}$ and 160.5 ± 55.8 HU for $VMI_{77keV}$) in the evaluated targets/OARs. In contrast, $VMI_{50keV}$ and $VMI_{77keV}$ provided equivalent HU values ($p$ = 0.07) for PTV for the prostate cases (25.5 ± 10.5 HU for the $VMI_{50keV}$ and 22.3 ± 6.9 HU for the $VMI_{77keV}$).

Fig. 5 illustrates the mean 3D–GPR derived from doses computed based on the LUTs generated using the large phantom size and those using the small phantom size. For both $TP_{50keV}$ and $TP_{77keV}$, the mean 3D–GPR with 1%/1 mm the criteria were > 90% for all evaluated structures, and the 3D–GPR was generally higher when doses were calculated by the AAA than AXB. In brain cases, the mean effect of the inaccurate HU estimation was significantly larger but statistically significant ($p$ < 0.05) in the $TP_{50keV}$ (the mean 3D–GPR was 98.3% and 97.3% for overall and PTV, respectively) than those in the $TP_{77keV}$ (the mean 3D–GPR was 99.5% and 99.4% for overall and PTV, respectively) when doses were calculated by the AXB.

Fig. 6 shows the absolute differences in the dosimetric parameters between treatment plans based on the LUTs acquired using different phantom sizes for PTV (Fig. 6a) and OARs (Fig. 6b). Except for prostate cases, the differences in the dosimetric parameters with $VMI_{50keV}$ for PTV (the maximum difference was 0.35 Gy for $D_{50\%}$ in brain case) were

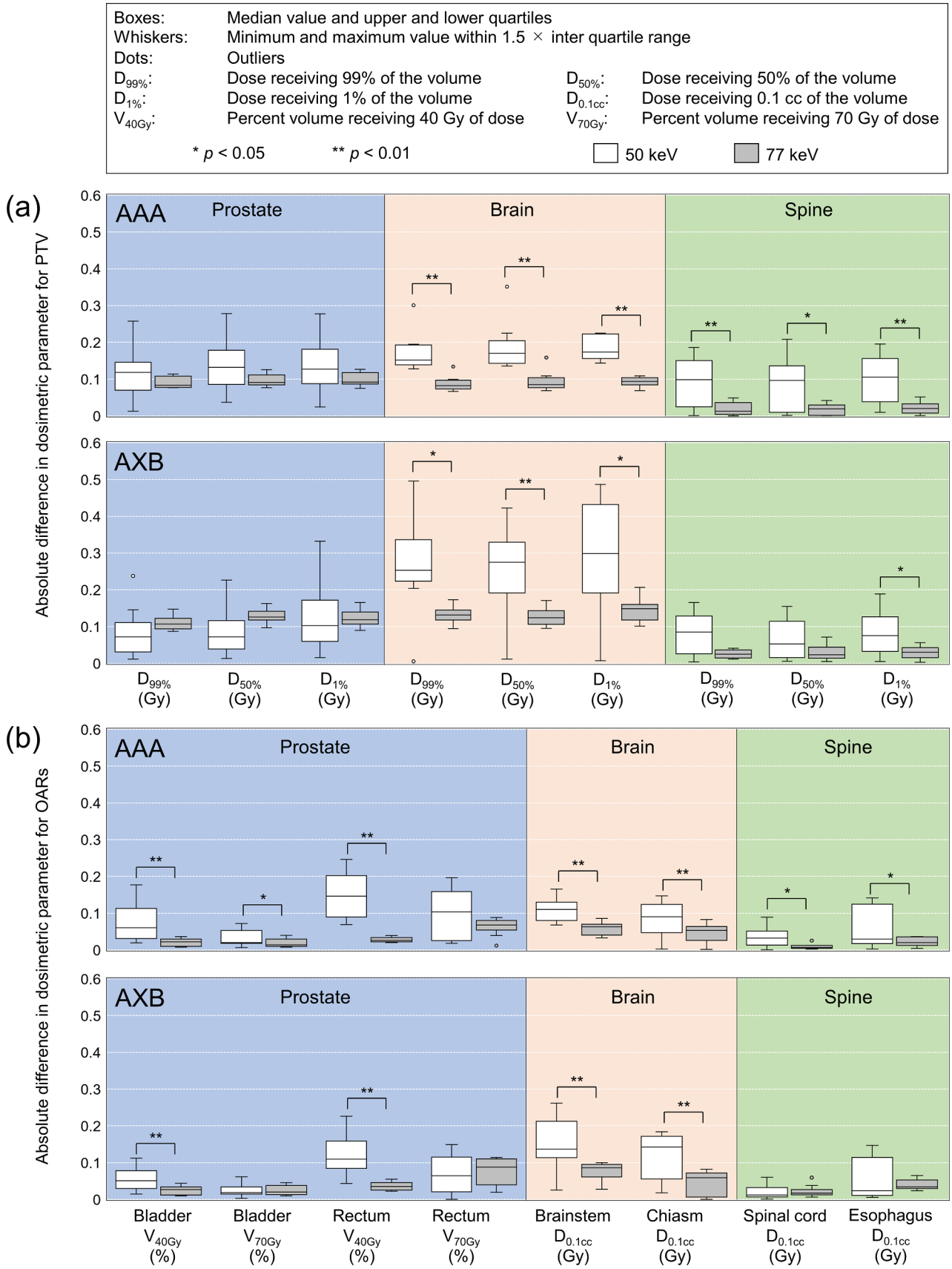


**Fig. 6.** Differences in the dosimetric parameters between the treatment plans using the LUTs acquired using different phantom sizes for the (a) PTV and (b) OARs.

slightly larger but statistically significant ($p < 0.05$) than the corresponding values with $VMI_{77keV}$ (the maximum difference was 0.16 Gy for $D_{50\%}$ in brain case) when AAA was used for treatment planning. When AXB was used, the differences for PTV varied widely in brain cases, and the maximum difference in dosimetric parameters with $VMI_{77keV}$ was 0.21 Gy ($D_{1\%}$) while that with $VMI_{50keV}$ was 0.5 Gy ($D_{99\%}$). For OARs, when $VMI_{77keV}$ was used for treatment planning, the mean effect of the inaccurate HU estimation was < 0.1 Gy (or < 0.1%) for all evaluated structures, and maximum difference was 0.12% for $V_{70Gy}$ for rectum in the prostate case with AXB. Generally, the differences in the dosimetric parameters with $VMI_{50keV}$ were slightly larger but statistically significant ($p < 0.05$) than the corresponding values with $VMI_{77keV}$.

## 4. Discussion

In this study, we demonstrated that the HU values in $VMI_{50keV}$ and SECT image varied depending on the volume of the surrounding materials and the scanning parameters, especially in the case of high-density materials (Figs. 2 and 3). Consequently, in our anthropomorphic phantom study, inaccurate HU estimation in the case of $VMI_{50keV}$ and SECT induced a larger dose deviation than the $VMI_{77keV}$ case (Fig. 4). In theory, the VMIs are less affected by the beam-hardening effect, which is recognized as one of the major concerns in terms of inaccurate HU measurement, and thus provide more accurate HU values than conventional single-energy CT scanners that use a polychromatic energy beam [12]. However, Goodsitt et al. reported that differences between measured and theoretical HU values was as high as 300 HU for $VMI_{50keV}$ in the case of a dense material (1.83 g/cm$^3$); thus, they concluded that monochromatic images were not truly monochromatic [8]. Moreover, the quantitative measurements of HU values in the $VMI_{50keV}$ and SECT image varied widely depending on the scanning protocols especially for high density materials in the large phantom (Fig. 3). Thus, the inaccurate HU estimation in the $VMI_{50keV}$ and SECT image may cause dosimetric errors in treatment planning procedure and the use of the $VMI_{77keV}$ for treatment planning can be feasible. We believe that understanding the performance of DECT scanners is imperative for creating suitable LUTs for treatment planning.

Zurl et al. varied the scanning protocols (tube voltage, tube current, reconstruction filter, etc.) using a conventional CT scanner (120 kVp) to generate 270 LUTs; then, they applied incorrect LUTs for brain radiotherapy treatment planning (20 patients received opposed field irradiation, 5 patients received orthogonal field irradiation, and 3 patients received intensity-modulated radiotherapy) [13]. Consequently, they observed that the mean increase in radiation dose was 0.7 ± 0.1% in the brain tissue, while it was 1.3 ± 0.4% in the bone. Tsukihara et al. utilized an anthropomorphic phantom and investigated the effect of inaccurate HU estimation in the case of the conventional CT scanner by varying the phantom size [14]; in their study, the difference in the dosimetric parameters (opposed field irradiation) using two different LUTs was limited (1.5%) in the lung tumor case, whereas it was up to 11.7% in the oral tumor case, wherein a high-density structure was involved in the PTV. To the best of our knowledge, our study is the first work to investigate the effect of inaccurate HU estimation of the VMI at low energy levels on dose distributions for VMAT treatment planning for patients with prostate cancer (large patient body), brain tumor (small patient body), and spine metastases (high-density target). In general, the difference in the 3D–GPR and dosimetric parameters between $TP_{50L}$ and $TP_{50S}$ was larger than those between $TP_{77L}$ and $TP_{77S}$, and the difference was more prominent for brain cases when AXB was used (the maximum difference was approximately 0.5 Gy for brain cases). Because the difference of 0.5 Gy was < 1% of the prescription dose (60 Gy), the effect of inaccurate HU estimation on the treatment planning based on the VMI at low energy levels might be clinically insignificant considering its advantage of improving the visibility of regions of interest to assist radiation oncologists. However, careful consideration is needed before clinical introduction especially for more sophisticated dose calculation algorithm, because the errors in dose calculations due to inaccurate HU estimation should not occur. Ideally, a large phantom should be used for generating the LUT for bigger treatment planning sites such as lung and pelvis, and a small one should be for head-and-neck and brain, which have smaller external contour.

However, there are several limitations to our study that warrant mention. First, the phantom used to simulate different phantom sizes was composed of homogeneous water-equivalent material; thus, various factors in the inhomogeneous environment of a real patient were not considered. Second, the effect of the contrast-enhanced agent on dose distribution is not investigated; in particular, the HU values in the case of the contrast-enhanced agent rapidly increases in the VMI at a low energy level because of K-shell photon absorption [4]; this difference in HU values between contrast-enhanced and unenhanced VMI might induce unexpected dose errors. Third, VMAT plans for patients were generated based on the $VMI_{50keV}$ and $VMI_{77keV}$, and the VMAT plans based on the SECT images could not be evaluated. Fourth, there are several acquisition techniques for dual-energy data using methodologies such as dual source and dual layer techniques, with each having inherent advantages and disadvantages [15,16]; thus, the accuracy of HU estimation might differ based on the DECT systems used. Finally, the effect of the inaccurate CT numbers on the accuracy of the dose delivery cannot be investigated. However, despite these limitations, the quantitative data obtained in our study provides important insights in the use of low-energy VMI for VMAT treatment planning.

In conclusion, the HU values measured using the fast kilovoltage switching DECT scanner varied depending on the volume of the surrounding material and the scanning protocols; in addition, the observed variation in the HU values was more prominent for high-density materials in the low-energy VMI. The maximum dosimetric error in VMAT planning caused by inaccurate HU estimation was 0.5 Gy (< 1% of the prescription dose) for $VMI_{50keV}$ when doses were calculated by the AXB. Though the dosimetric error may be clinically insignificant, it should not occur during the treatment planning procedure.

## Funding

This study was supported by JSPS KAKENHI Grant (Grant-in-Aid for Young Scientists (B) 17K15816).

## Conflict of interest

None.

## References

[1] Verbakel WFAR, Senan S, Cuijpers JP, Slotman BJ, Lagerwaard FJ. Rapid delivery of stereotactic radiotherapy for peripheral lung tumors using volumetric intensity-modulated arcs. Radiother Oncol 2009;93:122–4. https://doi.org/10.1016/j.radonc.2009.05.020.

[2] Quan EM, Li X, Li Y, Wang X, Kudchadker RJ, Johnson JL, et al. Clinical investigation: genitourinary cancer a comprehensive comparison of IMRT and VMAT plan quality for prostate cancer treatment. Int J Radiat Oncol Biol Phys 2012;83:1169–78. https://doi.org/10.1016/j.ijrobp.2011.09.015.

[3] Balaji K, Yadav P, BalajiSubramanian S, Anu Radha C, Ramasubramanian V. Hybrid volumetric modulated arc therapy for chest wall irradiation: for a good plan, get the right mixture. Phys Med 2018;52:86–92. https://doi.org/10.1016/j.ejmp.2018.06.641.

[4] Johnson TRC. Dual-energy CT: general principles. AJR Am J Roentgenol 2012;199:S3–8. https://doi.org/10.2214/AJR.12.9116.

[5] Ohira S, Wada K, Hirata T, Kanayama N, Ikawa T, Karino T, et al. Clinical implementation of contrast-enhanced four-dimensional dual-energy computed tomography for target delineation of pancreatic cancer. Radiother Oncol 2018. https://doi.org/10.1016/j.radonc.2018.01.012. in press.

[6] Wichmann JL, Nöske E-M, Kraft J, Burck I, Wagenblast J, Eckardt A, et al. Virtual monoenergetic dual-energy computed tomography: optimization of kiloelectron volt settings in head and neck cancer. Invest Radiol 2014;49:735–41. https://doi.org/10.1097/RLI.0000000000000077.

[7] Shuman WP, Green DE, Busey JM, Mitsumori LM, Choi E, Koprowicz KM, et al. Dual-energy liver CT: effect of monochromatic imaging on lesion detection,

conspicuity, and contrast-to-noise ratio of hypervascular lesions on late arterial phase. Am J Roentgenol 2014;203:601–6. https://doi.org/10.2214/AJR.13.11337.
[8] Goodsitt MM, Christodoulou EG, Larson SC. Accuracies of the synthesized monochromatic CT numbers and effective atomic numbers obtained with a rapid kVp switching dual energy CT scanner. Med Phys 2011;38:2222–32. https://doi.org/10.1118/1.3567509.
[9] Ohira S, Karino T, Ueda Y, Nitta Y, Kanayama N, Miyazaki M, et al. How well does dual-energy CT with fast kilovoltage switching quantify CT number and iodine and calcium concentrations? Acad Radiol 2018;25:519–28. https://doi.org/10.1016/j.acra.2017.11.002.
[10] Ohira S, Yagi M, Iramina H, Karino T, Washio H, Ueda Y, et al. Treatment planning based on water density image generated using dual- energy computed tomography for pancreatic cancer with contrast-enhancing agent: phantom and clinical study. Med Phys 2018;45:5208–17. https://doi.org/10.1002/mp.13180.
[11] Nelms BE, Opp D, Robinson J, Wolf TK, Zhang G, Moros E, et al. VMAT QA: measurement-guided 4D dose reconstruction on a patient. Med. Phys. 2012;39:4228–38. https://doi.org/10.1118/1.4729709.
[12] Yagi M, Ueguchi T, Koizumi M, Ogata T, Yamada S, Takahashi Y, et al. Gemstone spectral imaging: determination of CT to ED conversion curves for radiotherapy treatment planning. J Appl Clin Med Phys 2013;14:173–86. https://doi.org/10.1120/jacmp.v14i5.4335.
[13] Zurl B, Tiefling R, Winkler P, Kindl P, Kapp KS. Hounsfield units variations: impact on CT-density based conversion tables and their effects on dose distribution. Strahlenther Onkol 2014;190:88–93. https://doi.org/10.1007/s00066-013-0464-5.
[14] Tsukihara M, Noto Y, Sasamoto R, Hayakawa T, Saito M. Initial implementation of the conversion from the energy-subtracted CT number to electron density in tissue inhomogeneity corrections: an anthropomorphic phantom study of radiotherapy treatment planning. Med Phys 2015;42:1378–88. https://doi.org/10.1118/1.4908207.
[15] Pelgrim GJ, van Hamersvelt RW, Willemink MJ, Schmidt BT, Flohr T, Schilham A, et al. Accuracy of iodine quantification using dual energy CT in latest generation dual source and dual layer CT. Eur Radiol 2017;27:3904–12. https://doi.org/10.1007/s00330-017-4752-9.
[16] Sakabe D, Funama Y, Taguchi K, Nakaura T, Utsunomiya D, Oda S, et al. Image quality characteristics for virtual monoenergetic images using dual-layer spectral detector CT: comparison with conventional tube-voltage images. Phys Med 2018;49:5–10. https://doi.org/10.1016/j.ejmp.2018.04.388.